Research Square

Preprints are preliminary reports that have not undergone peer review.
They should not be considered conclusive, used to inform clinical practice,
or referenced by the media as validated information.

Synthetic cannabinoid JWH-018 increases α-Synuclein toxicity by ubiquitin-proteasome system impairment

Carla Ferreira
Centro de Investigação Interdisciplinar Egas Moniz
Rui M. Almeida
Centro de Investigação Interdisciplinar Egas Moniz
Sandra Tenreiro
Universidade Nova de Lisboa
Alexandre Quintas
aquintas@egasmoniz.edu.pt

Centro de Investigação Interdisciplinar Egas Moniz

Article

Keywords: Saccharomyces cerevisiae, cannabinoid, alpha-synuclein (α-synuclein), ubiquitin-proteasome system

Posted Date: October 22nd, 2026

DOI: https://doi.org/10.21203/rs.3.rs-11064598/v1

License: This work is licensed under a Creative Commons Attribution 4.0 International License.
Read Full License

Additional Declarations: No competing interests reported.

Synthetic cannabinoid JWH-018 increases α-Synuclein toxicity by ubiquitin-proteasome system impairment

Carla Ferreira[1†], Rui M. Almeida[1†], Sandra Tenreiro[2,*] and Alexandre Quintas[1,3*]

[1] Forensic Biochemistry and Toxicology Laboratory, Egas Moniz Center for Interdisciplinary Research (CiiEM); Egas Moniz School of Health & Science, Campus Universitário, Quinta da Granja, 2829-511 Caparica, Almada, Portugal; ciiem@egasmoniz.edu.pt

[2] iNOVA4Health, NOVA Medical School|Faculdade de Ciências Médicas, NMS|FCM, Universidade Nova de Lisboa; 1169-056 Lisboa, Portugal. stenreiro@nms.unl.pt

[3] Laboratório de Ciências Forenses e Psicológicas Egas Moniz, Campus Universitário – Quinta da Granja, Monte de Caparica, P-2825-084 Caparica, Portugal; lcforenses@egasmoniz.edu.pt

[†] Both authors contribute equally to the final manuscript

***** Correspondence: aquintas@egasmoniz.edu.pt; stenreiro@nms.unl.pt

Running title: Synthetic cannabinoid increases α-Synuclein toxicity

Keywords: *Saccharomyces cerevisiae*, cannabinoid, alpha-synuclein (α-synuclein), ubiquitin-proteasome system

Abstract

The aggregation and accumulation of α-synuclein (αSyn) in dopaminergic neurons is a hallmark of Parkinson's disease (PD), and its cellular clearance is essential for preventing neurotoxicity. This process relies heavily on the ubiquitin-proteasome system (UPS) and autophagy-lysosome mediated clearance, two critical pathways for degrading misfolded or damaged proteins. The contemporary trend of synthetic cannabinoid recreational use raises important questions about their potential effects on these crucial cellular mechanisms. In this study, we used a yeast model (*Saccharomyces cerevisiae*) to investigate the impact of the synthetic cannabinoid JWH-018 on αSyn-induced toxicity. Our findings reveal that JWH-018 significantly increases cellular toxicity caused by αSyn, and that this effect is mediated by UPS impairment. Treatment with JWH-018 led to a marked reduction in proteasome activity, which compromised the cell's ability to clear toxic protein aggregates. Our results provide a cellular and mechanistic link between synthetic cannabinoid exposure and the exacerbation of αSyn toxicity. These findings suggest a potential neurodegenerative risk associated with JWH-018, and highlight the

importance of further research into the effects of synthetic cannabinoids on cellular protein quality control systems.

Introduction

Parkinson's disease (PD) is the second most common neurodegenerative disease worldwide, characterised by the progressive, irreversible loss of dopaminergic neurons in the *substantia nigra pars compacta* (SNpc) region of the brain, with subsequent loss of control of motor functions leading to motor symptoms such as resting tremor, bradykinesia, postural instability, and muscular rigidity [1,2]; the cholinergic nervous system (related to cognitive impairment), the noradrenergic nervous system, and the serotonergic nervous system (related to depression and anxiety) are also impacted in PD [3]. Together with dementia with Lewy bodies (DLB), and multiple system atrophy (MSA), PD is a part of the synucleinopathy group of neurodegenerative syndromes [4], which are characterised at the molecular level by the presence of α-synuclein (αSyn) aggregates in cytoplasmic inclusions commonly known as Lewy bodies (LBs). αSyn, like βSyn and γSyn, is a member of the synuclein family of intrinsically disordered proteins. The 140-amino-acid αSyn protein is encoded by the *SNCA* gene, and is particularly abundant in the brain, specifically enriched in presynaptic terminals of neurons [5]. αSyn is associated with familial forms of PD via point mutations, single-nucleotide polymorphisms, or gene duplication or triplication events [6,7]. It is also a major component of LBs and Lewy neurites, present in many neurodegenerative diseases. The protein can bind a wide range of interactors, including other αSyn molecules, other synucleins, lipids, synaptic vesicles, and synapsins [8]. Although its physiological role remains under debate – trafficking and recycling of neurotransmitter-loaded vesicles, regulation of dopamine synthesis via histone binding, activation of nuclear receptors,

among others – its toxic role is far better understood [9][10]. Moreover, αSyn is reported to exist in a few different states: from monomers to tetramers, to oligomers, protofibrils, and fibrils [11], with the monomeric form assumed to be the most common state in pre-synapses and nuclei; oligomers and fibrils are associated with pathological states, including changes in cellular lipid homeostasis [11,12], dysregulated intracellular iron homeostasis causing iron-dependent lipid peroxidation (ferroptosis) [13], and gut microbiome dysbiosis, affecting the gut-brain axis. Moreover, current thinking links PD development to αSyn loss-of-function rather than gain-of-function [14].

Given the increase in the worldwide population, the increase in the lifespan, and the environmental stress of contemporary societies, associated with the lack of a cure or a disease-modifying therapy as an efficient means to slow down its progression, the burden of PD has increased dramatically over the past generation, overwhelming both families and healthcare and health support systems [15]. Current research focuses on promising disease-modifying pharmacological interventions that target inhibition of αSyn aggregation and extracellular propagation [16], enhance αSyn clearance, or inhibit of its production [16]. Nevertheless, most of these interventions are still in phase I/phase II clinical trials. As such, given the current panorama, many PD patients have turned to other means of managing disease-related symptoms. With the recent legalisation of cannabis products for medicinal and personal use in some parts of the world, many PD patients report their use in symptom management (namely, non-motor symptoms such as sleep, pain, or anxiety disorders), albeit with a variety of effects and outcomes [17,18]. Natural phytocannabinoids such as Δ^9-Tetrahydrocannabinol (THC) and cannabidiol (CBD) can exert antagonistic effects [19] – although with a prevalence towards improvement of locomotor activity, and decrease of inflammation, microglial/astrocyte

activation, and oxidative stress in animal models of PD [20], whereas the effect of synthetic cannabinoids (SCs) - a group with similar properties to Δ^9-THC and other cannabinoids naturally found in the *C. sativa L.* plant [21] - is still poorly characterised.

SCs show affinity for cannabinoid receptors CB_1R and CB_2R, which are part of the endocannabinoid system and have anti-inflammatory, antioxidant, and pro-neurogenic properties, making them potential targets for reducing the symptoms of several neurodegenerative conditions in humans [22–25]. The existence of two distinct endocannabinoid receptors, CB_1R and CB_2R, their distribution across different brain regions, and the distinct cellular-level responses they elicit upon activation suggest a possible neuroprotective role for cannabinoids. Evidence supporting the endocannabinoid system's involvement in PD indicates that both CB1R and CB2R activation may contribute to neuroprotection [20]. Moreover, phytocannabinoids seem to exert a protective effect on PD, either by binding to CB_1R, inhibiting dopamine beta-hydroxylase activity and decreasing glutamate levels, or by binding to CB_2R, reducing neuroinflammation [26]. Nevertheless, the endocannabinoid system has also been implicated in neurodegenerative processes [27].

Among the known synthetic cannabinoids, JWH-133, a potent CB_2R agonist, exhibited neuroprotective activity in a MPTP (1-methyl-4-phenyl-1,2,3,6-tetrahydropyridine) model of PD [28]. However, other SCs exhibit different properties that have not yet been fully studied. Additionally, more recent synthetic cannabinoids display higher affinity towards CB_1R and CB_2R, which strongly activate the brain reward pathways and expose the user to a higher risk of developing severe illnesses, including psychosis [29]. Hence, the recentness of the NPS trend – it originated in the early 2000s [30] – hinders a full understanding of the impact of their consumption in PD. NPS properties and their long-term effects remain poorly characterised. Nonetheless, the limited literature on these new

112 substances suggests a trend towards neurotoxicity [31–44]. Thus, the hypothesis of these
113 substances being implicated in PD onset cannot be discarded, especially knowing that
114 according to the European Union Drugs Agency (EUDA), NPS seizures are dominated
115 by SCs and synthetic cathinones [45].
116
117 In this paper, we focus on JWH-018 (naphthalen-1-yl(1-pentyl-1H-indol-3-
118 yl)methanone, also known as AM678), one of the earliest synthetic cannabinoids found
119 in herbal mixtures sold in Smart Shops and the first to be controlled, to study its influence
120 on αSyn aggregation using *Saccharomyces* (*S.*) *cerevisiae* expressing αSyn as a
121 humanised yeast model of PD. These misfolding disease yeast models have been
122 extensively used to clarify the fundamental mechanisms and pathways underlying PD
123 [46–48]. Although developing accurate PD models (at the cellular or organism level) has
124 been challenging, current models based on overexpression of PD-associated proteins such
125 as αSyn are robust enough to answer specific scientific questions [49]. Previously, we
126 showed that JWH-018 increases glycolytic flux, which fuels cell growth at the expense
127 of the pentose phosphate pathway [50]. Since the latter is responsible for the generation
128 of NADPH, which provides reducing power to deal with oxidative stress conditions, and
129 given that the generation of Reactive Oxygen Species (ROS) in brain cells arises mainly
130 from dopamine metabolism, a decrease in NADPH over a long period of time as a
131 consequence of SC consumption may contribute to PD onset [51].

132 Overall, the present work aimed to assess molecular and cellular toxicity and risks
133 associated with the long-term effects of the synthetic cannabinoid JWH-018 exposition,
134 namely, to determine the cytotoxic, molecular, αSyn clearance, and autophagy effects of
135 this SC using a yeast PD model. We observed increased αSyn toxicity, reduced final
136 biomass, increased αSyn protein levels and increased formation of αSyn-GFP inclusions

in yeast cells expressing an αSyn-GFP fusion protein treated with JWH-018. The dysregulation of αSyn clearance was evaluated and ascribed to the ubiquitin-proteasome system.

Results

Cytotoxicity assays

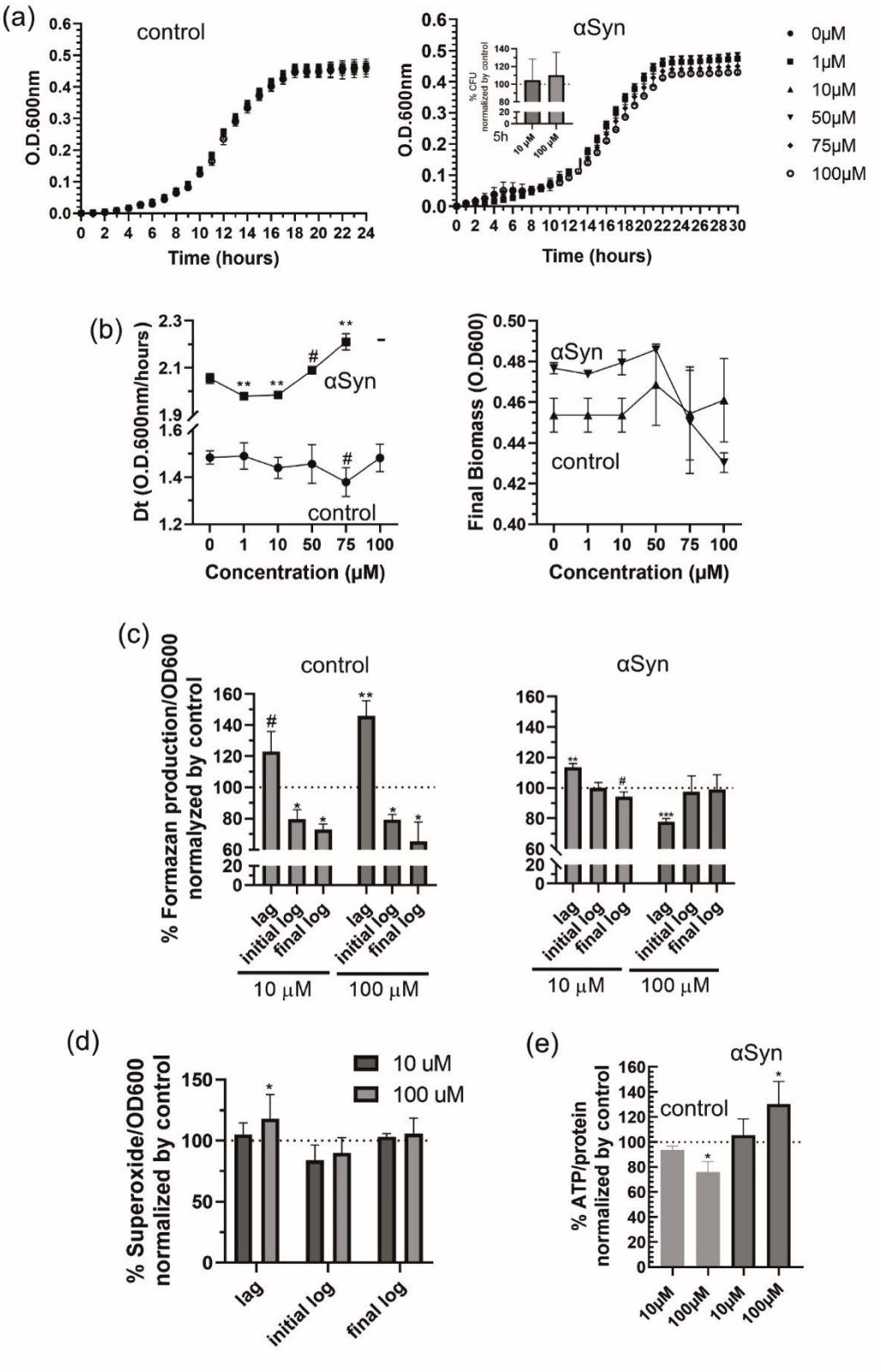
To investigate the effect of JWH-018 on a cellular model of PD, yeast cells expressing human αSyn in fusion with a GFP reporter (αSyn-GFP) [52] were exposed to increasing concentrations (0, 1, 10, 50, 75 and 100 μM) of the SC (Fig. 1). Cell growth was monitored by optical density at 600 nm over a 30-h or 24-h time frame for cells expressing αSyn or for the control cells carrying the empty vector (Fig. 1a). For the latter, the growth curve kinetics were not altered by incubation with JWH-018 at any of the concentrations tested. Conversely, cellular growth changed in a JWH-018 concentration-dependent manner in the presence of overexpressed αSyn. At 100 μM of JWH-018, growth differences can be observed: the compound promotes an increase in growth rate at 5 h, resulting in a new lag phase and a lower final biomass. To evaluate this initial effect, the number of colony-forming units (CFU) was assessed at 5h. No statistically significant differences in the number of viable cells were observed (Fig. 1a). To understand further putative differences between yeast growth rates in the presence and absence of JWH-018, the curves were fitted to a logistic equation, which allows for retrieving the final biomass and doubling time values (Fig. 1b). The SC yielded no observable effect on growth kinetics in cells not expressing αSyn, but affected duplication times in αSyn-expressing cells; the estimated average value for duplication time was 2.055 ± 0.022 hours in the absence of JWH-018, which decreased significantly by 0.075 ± 0.013 and 0.070 ± 0.014 h for cells incubated with 1 μM ($P<0.02$) or 10 μM ($P<0.02$) of JWH-018, respectively. Conversely, the duplication time upon incubation with 75 μM of the compound increased significantly by 0.034 ± 0.016 hours ($p<0.02$); the duplication time also seems to increase in the presence of 100 μM of JWH-018, compared to the

control – nevertheless, its value could not be obtained since the logistic equation did not fit the growth curve data. The final biomass for the untreated cells overexpressing αSyn shows an estimated average value of 0.477 ± 0.003 $O.D._{600nm}$, which increases by 0.009 ± 0.002 ($P<0.02$) in the presence of 50 μM of JWH-018, and decreases by 0.026 ± 0.015 ($P<0.02$) and by 0.046 ± 0.003 $O.D._{600nm}$ ($P<0.001$) upon incubation with 75 μM or 100 μM of JWH-018, respectively.

To further assess these results, mitochondrial activity (Fig. 1c) and superoxide levels (Fig. 1d) were evaluated in control and αSyn-expressing yeast cells exposed to different concentrations of JWH-018 at three different stages of the growth phase: lag phase, initial log phase, and final log phase. Exposure to 10 or 100 μM JWH-018 impacted all time points studied compared to untreated cells, namely: an increase in lag phase (23.0 ± 8.8 %, $P<0.1$), and a significant decrease in the initial (-20.5 ± 5.7 %, $P<0.05$) and final log phases (-27.1 ± 7.3, $P<0.05$) upon incubation with 10 μM JWH-018; and a significant increase in the lag phase (45.0 ± 7.4 %, $P<0.02$), and significant decreases in the initial (-20.7 ± 4.9 %, $P<0.05$) and final log phases (-34.6 ± 10.0, $P<0.05$) upon incubation with 100 μM JWH-018. Moreover, αSyn-expressing yeast cells showed a significant increase in mitochondrial activity during the lag phase (13.6 ± 1.8 %, $P<0.02$) in the presence of 10 μM of JWH-018, which subsequently decreased until reaching the final log phase (-5.8 ± 2.5 %, $P<0.1$). However, αSyn-expressing yeast cells incubated with 100 μM JWH-018 showed a significant decrease in mitochondrial activity during the lag phase (-22.1 ± 1.7 %, $P<0.001$). To complement the mitochondrial activity evaluation in the presence of the SC, the superoxide content was measured (Fig. 1d). Exposure to different concentrations of JWH-018 showed a significant positive correlation in superoxide

188 concentration, with a reported increase of 14.6 ± 5.06 %, ($P<0.05$) in αSyn-expressing
189 cells during the lag phase.

190 ATP levels were also assessed, since the literature reports that ATP levels change
191 during the final log phase in the presence of JWH-018 [53]. The results showed that, upon
192 treatment with JWH-018, ATP levels increase in αSyn-expressing cells and decrease in
193 cells transformed with the empty vector. Thus, compared to the untreated control, cells
194 not expressing αSyn showed a decrease in ATP levels of 24.2 ± 5.9 % ($P<0.05$), whereas
195 cells expressing αSyn increased ATP levels by 30.4 ± 10.8 % ($P<0.05$) when treated with
196 100 μM JWH-018 (Fig. 1e).
197



198

199 Fig 1- JWH-018 toxicity assays on *S. cerevisiae* BY4741 cells harboring vector p426Gal-αSyn-GFP
200 or p426Gal (A) Growth curves of *S. cerevisiae* exposed to different concentrations of JWH-018. Inset
201 represents the percentage of CFU of αSyn-expressing cells treated with different concentrations of

JWH-018 after 5 hours of growth, compared to untreated cells (B) growth curves were fitted to the standard form of the logistic equation which allowed an estimation of the final biomass and doubling time values (Dt) from the growth rate using the formulae Ln2/r;●,▲: cells transformed with the p426Gal vector; and ■,▼: cells transformed with the p426Gal-αSyn-GFP vector. (C) Mitochondrial activity and (D) superoxide quantification in the presence of 10 and 100μM of JWH-018 during the lag, initial log, and final log phases. (E) ATP quantification in the presence of 10 and 100μM of JWH-018. Values represent the mean ± SD, and the representative result is shown from at least three independent experiments. **p<0.02; *p<0.05 and #p<0.1.

Studying the effect of JWH-018 on yeast PD model cells

JWH-018 was shown to be toxic to yeast cells expressing αSyn at the highest concentration tested herein. To further understand the impact of this compound in the yeast PD model, fluorescence microscopy was performed to observe changes in αSyn inclusions (namely, intracellular localisation and percentage of affected cells) using the αSyn-GFP reporter fusion protein. After 14h of αSyn-GFP expression, 62.9 ± 2.2% of untreated yeast cells exhibited inclusions, whereas in cells treated with 100 μM JWH-018, that value increased to 78.2 ± 1.0 % . Fluorescence microscopy showed that incubation with 100 μM of JWH-018 increased the number of cells presenting αSyn inclusions by 15.3 ±1.4 % (P<0.001) (Fig. 2a). These observations were corroborated by quantifying αSyn-GFP levels via western blot densitometry analysis of protein extracts after 14 hours of cell growth, using an anti-αSyn antibody. αSyn phosphorylation at position S129 – a recognised marker of oligomerisation [54] – was also assessed with a specific antibody against this post-translational modification. Pgk1 was used as loading control. Normalising the values to 0 μM, incubation with 100 μM of JWH-018 yielded a significant increment of αSyn-GFP levels of 1.212±0.078 (P<0.05) – a 21% increase (Fig.

2b). Phosphorylation also increased 24% (1.238±0.188) when compared to the control; however, this increment was due to the increase of total αSyn (1.028±0.195) (Fig. 2b). Thus, phosphorylation of αSyn at position S129 does not seem to be affected by incubation with JWH-018.

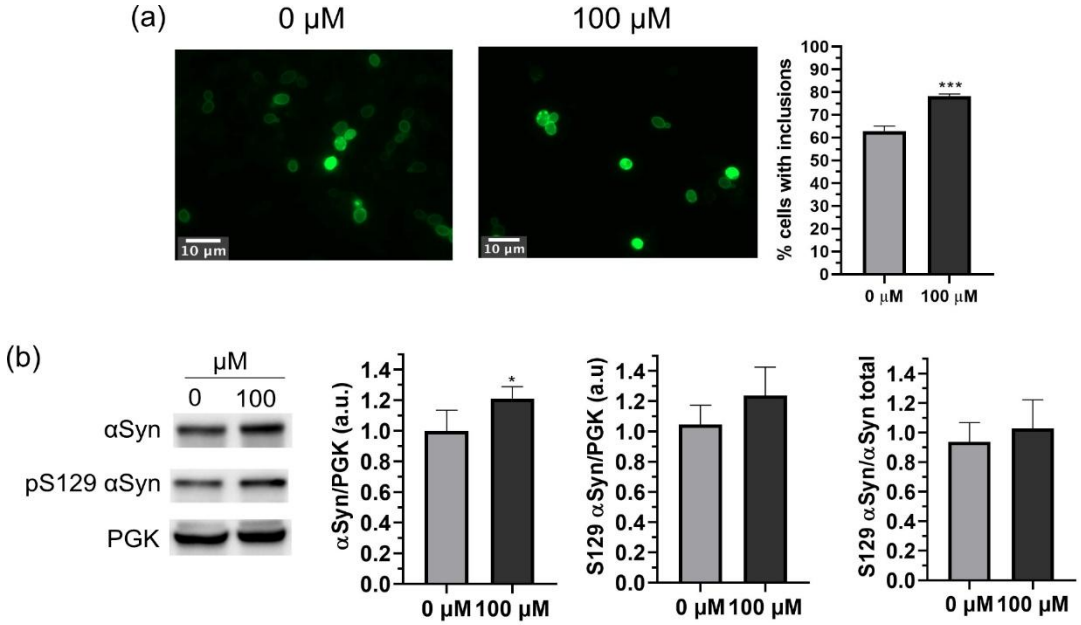


Fig 2 - Cellular impact of JWH-018 on the toxicity of αSyn. (A) Intracellular localisation of WT αSyn-GFP, and percentage of BY4741 WT yeast cells containing αSyn-GFP inclusions, assessed by fluorescence microscopy after 14 hours of αSyn-GFP expression induction (*** $p<0.001$) (left panel), and the corresponding quantification of the percentage of cells with inclusions (right panel). (B) Total and S129-phosphorylated αSyn protein levels were quantified by western blot analysis of total protein extracts after 14h of αSyn-GFP expression (left panel). Densitometric analysis of the immunodetection assay was expressed by the ratio between αSyn and Pgk1 (αSyn/PGK; left panel); S129-αSyn and Pgk1 (S129 αSyn/PGK)– middle panel; and S129-αSyn levels normalised to the total αSyn levels (S129 αSyn/αSyn total; right panel). The representative results are calculated as the average of a minimum of three replicates. Values represent the mean ± SD. (*$p<0.05$). In (B), αSyn,

pS129-αSyn and Pgk1 were detected on separate membranes loaded with the same protein extracts and processed in parallel; each strip shows two adjacent lanes cropped from a single membrane, and strips from different membranes are separated by white space. Full-length blots are presented in Supplementary Fig. S1.

αSyn clearance in the presence of JWH-018

A clearance assay was performed to assess whether higher levels of αSyn in the presence of 100 μM JWH-018 stemmed from a decrease in αSyn-GFP clearance. To this purpose, a clearance assay was performed by inducing αSyn-GFP expression for 14 hours, followed by replacement of galactose with glucose (to repress the GAL1 promoter and stop gene expression (57)) and incubation with 100 μM of JWH-018. αSyn-GFP clearance assay was followed for 12 hours by quantifying protein levels via western blot densitometric analyses after 0, 6, 9, and 12 h of clearance (Fig. 3a). αSyn-GFP levels were 0.470±0.072, 0.161±0.066 and 0.105±0.038 in untreated cells, and 0.4071±0.077, 0.247±0.053 and 0.105±0.059 in cells incubated with 100 μM JWH-018, at the 6, 9 and 12h timepoints, respectively. This indicates a putative higher αSyn level in the presence of JWH-018 when compared to control at time 9h ($p<0.1$) (Fig. 3a). Subsequently, clearance kinetics were plotted, and the result was fitted to a one-phase decay equation [55] (Fig. 3b). The calculated clearance rates were 0.084±0.015 (R^2 = 0.9302) and 0.111±0.037 (R^2 = 0.9377), for cells incubated with 0 and 100 μM of the SC, respectively. Thus, αSyn-GFP clearance seems to decrease in the absence of the synthetic cannabinoid, albeit without statistical significance. Moreover, detailed analysis of the plot shows a higher clearance rate between 0 and 6h upon incubation with 100 μM JWH-018, at which point the trend inverts over the next time interval (6-9h). Therefore, a bar chart was plotted with the differences in αSyn-GFP levels in the Δ6-0, Δ9-6 and Δ12-9 time

intervals (Fig. 3c). We observed a statistically significant difference in αSyn-GFP decrease in the presence of 100 μM of JWH-018 at time interval Δ9-6, which only decreased by 16 ± 7% (P<0.02), in contrast with 31±3% in untreated cells. This alteration in αSyn-GFP clearance in the presence of the SC can justify the increment of αSyn protein levels.

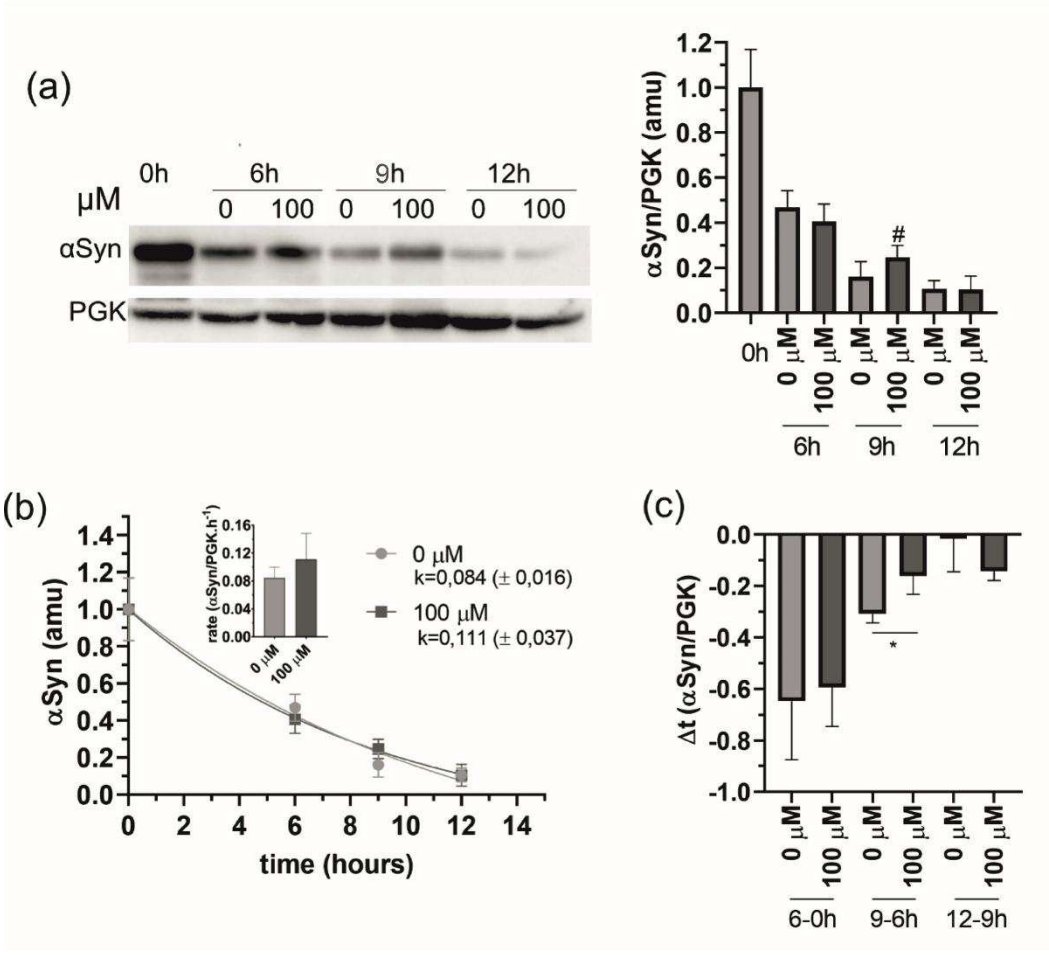


Fig 3 - JWH-018 affects αSyn-GFP clearance. (A) Clearance evaluated by αSyn-GFP protein levels at time points 0, 6, 9, and 12h, assessed by western blot (left panel); densitometric analysis of the immunodetection of αSyn relative to Pgk1, resulted in the possible decrease of the clearance rate of αSyn levels in the presence of 100 μ JWH-018 at time 9h (#p<0.1) (right panel). (b) The kinetic degradation curve of αSyn suggests a possible increase in the clearance rate of protein levels in JWH-018 presence when fitted to a one-phase exponential decay. (c) Delta time points of αSyn clearance, resulting in a decrease of

protein clearance at time interval Δ9-6 in the presence of 100 μM of JWH-018 (*p<0.05). Each result represents the average of three independent experiments. Values represent the mean ± SD. In (A), αSyn and Pgk1 were detected on separate membranes loaded with the same protein extracts and processed in parallel; each strip shows seven adjacent lanes cropped from a single membrane, and strips from different membranes are separated by white space. Full-length blots are presented in Supplementary Fig. S2.

JWH-018 effect on the Proteasome and Autophagy-mediated clearance of αSyn

The reduction of αSyn-GFP clearance in the presence of JWH-018 could stem from a dysfunction of the cellular mechanisms involved in αSyn clearance, possibly implicating the ubiquitin-proteasome system (UPS) and/or autophagy mechanisms. To evaluate the impact of JWH-018 on αSyn-GFP clearance, an assay using 100 μM of this synthetic cannabinoid was performed in cells co-expressing αSyn and GFPu, an unstable GFP reporter consisting of a fusion of GFP with a constitutive degradation signal (CL-1) that promotes its rapid degradation by the UPS [56]. GFPu and αSyn levels were assessed by western blot after 14 h and 18 h of cell growth, using anti-GFP and anti-αSyn antibodies, with Pgk1 as loading control. Cells incubated with 100 μM of JWH-018 yielded GFPu levels of 4.37 ± 1.76 after 14 h, a significant increment of 340 ± 110 % (P<0.05) compared to that of untreated cells (Fig. 4a). The results obtained at 18h, despite exhibiting an increasing trend, did not show statistically significant differences between 0μM and 100 μM (1.00 ± 0.66 vs 1.27 ± 0.32). Likewise, αSyn levels at time point 14h show an increasing trend, albeit without statistical significance, between 0μM and 100 μM (1.00 ± 0.58 vs 2.31 ± 1.32). However, at 18 h, the results in the presence of 100 μM of JWH-018 – 2.17 ± 0.28 – were statistically significant, corresponding to an increment of αSyn protein levels of 117 % ± 40.1 % (P<0.05) (Fig. 4a). To corroborate the observed

GFPu protein increment in the presence of 100 μM of JWH-018, GFPu fluorescence emission was monitored by spectrofluorescence at the 14h time point. Cells incubated with JWH-018 exhibited an increment in GFPu fluorescence of 43.1±17.57 % ($P<0.02$) compared to the control (untreated cells) (Fig. 4b). The accumulation of GFPu observed in the western blot and fluorescence assays point towards an impairment of the ubiquitin-proteasome system in the presence of 100 μM of JWH-018, leading to the accumulation of αSyn.

Autophagy was also investigated to obtain a more complete picture of the mechanisms underlying αSyn accumulation in the presence of JWH-018, using GFP-Atg8 as a reporter, and a starvation condition as a positive control [57,58]. Atg8 is one of the key molecules involved in autophagy, since it conjugates to phosphatidylethanolamine on the autophagic membrane, an essential step in autophagosome formation in eukaryotes [59][60] The study of Atg8 induction and autophagic flux were assessed by western blot after 14 hours of cell growth, via an anti-GFP antibody, using Pgk1 as loading control (fig 4c). Incubation with 100 μM of JWH-018 slightly decreased Atg8 induction by 7.6% (0.924±0.300, normalised to the absence of the cannabinoid), whereas the positive control – yeast cells transformed overexpressing GFP-Atg8 only and not exposed to the SC - increased it by 28% (1.281 ± 0.308) (Fig. 4c). Furthermore, autophagic flux was also assessed compared to the untreated control, reaching 0.845 ± 0.318 for the 100 μM JWH-018 incubation assay, and 2.215 ± 0.523 for the positive control assay – a decrease of 15.5% ± 5.8% and an increase of 122 ± 28 % ($P<0.01$), respectively. These results suggest a decreasing trend in Atg8 induction and autophagic flux in cells overexpressing αSyn in the presence of SC, although the differences were not statistically significant. αSyn levels were also compared between the different autophagy assays, with values normalised to untreated cells, reaching 3.532 ±

1.333 in the 100 µM JWH-018 incubation assay, and 0.465 ± 0.163 for the positive control compared to untreated cells, indicating a significant increase of αSyn levels in the presence of JWH-018 (253±67.9 %, P<0.02), and a decrease under the starvation condition (-53.5 ± 15,2 %, P<0.05). Thus, the results point towards a slight, but statistically insignificant, decrease in autophagic flux in the presence of 100 µM of JWH-018.

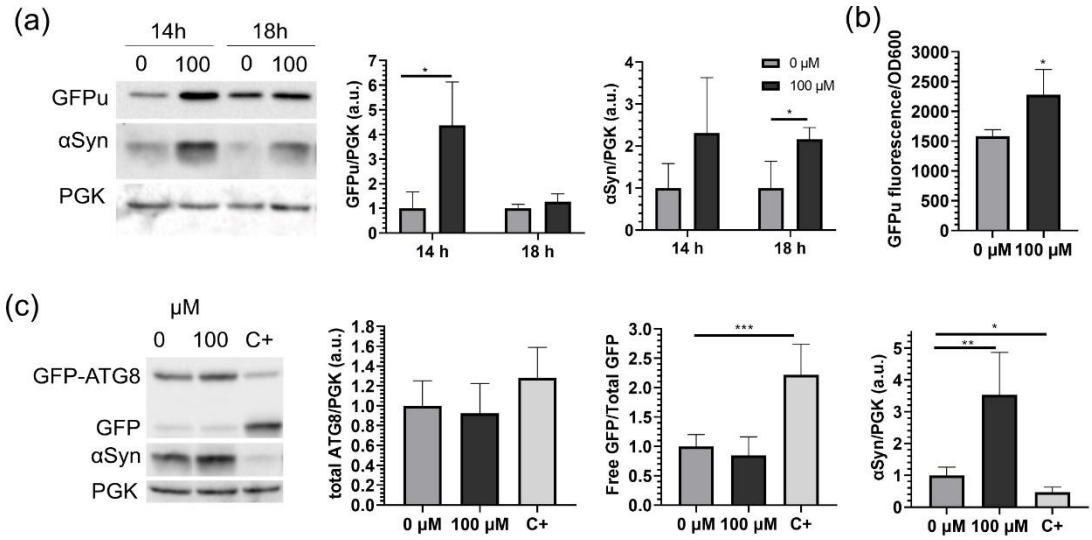


Fig 4 - The JWH-018 impact on cellular protein degradation mechanisms. (A) GFPu and αSyn protein levels were evaluated by western blot analysis of total protein extracts at 14h and 18h (left panel), and their densitometric analysis relative to the loading control (Pgk1), resulting in the accumulation of GFPu and αSyn in the presence of 100 µM of JWH-018 (*p<0.05) (right panel). (B) Spectrofluorometry of GFPu fluorescence shows a statistically significant accumulation of GFPu in the presence of 100 µM of JWH-018 (*p<0.05). (C) Autophagy evaluation via GFP-Atg8 protein levels calculated by western blot densitometric analysis of total protein extracts at 14h post-αSyn overexpression induction (left-hand panel), and densitometric analysis of the immunodetection of GFP and αSyn relative to Pgk1 (right-hand panel). Representative results are the average of three independent experiments. C+: Positive control. Values represent mean ± SD. *p<0.05, **p<0.02; ***p<0.01 In (A) and (C), GFP (GFPu or

GFP-Atg8/free GFP), αSyn and Pgk1 were detected on separate membranes loaded with the same protein extracts and processed in parallel; GFP-Atg8 and free GFP in (C) were detected on the same membrane. Each strip shows adjacent lanes cropped from a single membrane (four lanes in A, three lanes in C), and strips from different membranes are separated by white space. Full-length blots are presented in Supplementary Figs. S3 (A) and S4 (C).

Discussion

Since their first appearance in the drug market, synthetic cannabinoids have been the focus of UNODC alerts and global research due to the severe acute public health issues associated with them [61,62]. However, many consumers of these substances do not manifest acute health issues, but may suffer from long-term health issues that have not been observed yet, owing to the recentness of the problem. This work aimed to assess the molecular and cellular toxicity of synthetic cannabinoids, as well as the risks associated with their long-term effects, using JWH-018, the first SC found on the drug market, in a yeast model of PD, which is widely used to study the fundamental mechanisms and pathways underlying the disease.

We observed that JWH-018 at medium to high concentrations increased αSyn-GFP levels in cells expressing this fusion protein, compared with the untreated control. Interestingly, at low concentrations (1-10 μM), JWH-018 appears to benefit cells expressing αSyn-GFP by decreasing duplication time and/or increasing final biomass. This decrease in duplication time after exposure to low concentrations of JWH-018 was previously described in the literature and stems from increased glycolytic flux at the expense of decreased pentose phosphate pathway activity, driven by modulation of enzymes implicated in both pathways [53]. Moreover, a previous study in human SH-SY5Y cell lines showed a beneficial – though statistically insignificant – effect of JWH-018 in cell viability in concentrations up to 100 μM [63]. Sezer *et al.* did not observe

differences in cell viability in the same cell line in the presence of JWH-018, despite significant levels of oxidative stress [64]. However, a toxic impact on growth kinetics in yeast cells expressing αSyn-GFP was observed in the presence of 50-100 μM of JWH-018, since both growth rate and final biomass decreased. Previous studies [53,64] suggest that the adverse effect of exposure of cells expressing αSyn-GFP to 100 μM JWH-018 could arise from a decrease in the pentose phosphate pathway, which is critical for dealing with oxidative stress [53]. Furthermore, incubation with JWH-018 decreased cellular ATP content, a consequence of the growth rate increasen the presence of this synthetic cannabinoid [53]. This decrease was also observed in the present study in control cells not expressing αSyn-GFP. However, the presence of αSyn-GFP yielded higher levels of ATP when cells were exposed to 100 μM of JWH-018. Nevertheless, in the presence of galactose, ATP production results largely from respiratory chain activity [65]. We also observed a decrease in mitochondrial activity during the lag phase, suggesting an increase in the glycolytic pathway in this phase. After this initial growth phase, the mitochondrial activity in treated cells exhibits the same behaviour as the control culture.

Since JWH-018 at a concentration of 100 μM was toxic in the yeast PD model, fluorescence microscopy was used to understand the effect of this SC on αSyn inclusions. Results show a significant increment of 15.3±1.4 % ($P<0.001$) of cells exhibiting αSyn inclusions after 14 h of αSyn-GFP expression in the presence of 100 μM JWH-018 (Fig. 2a). As shown previously, both for this PD model as well as for others, αSyn aggregation increases with αSyn protein levels [66–68]. Therefore, we assessed whether the increment in inclusion body formation was solely due to increased levels of αSyn-GFP. Moreover, we also investigated the phosphorylation of αSyn-GFP at S129, since this post-translational modification of αSyn has been observed in LBs [69]. After 14 hours of cell

405 growth, western blot analysis showed a significant increment of αSyn protein levels
406 ($P<0.05$) (Fig. 2). However, the rate of phosphorylation of αSyn at position S129 does
407 not seem to be affected by JWH-018.

408 Some studies indicate that one of the molecular contributors to PD pathogenesis is
409 an inefficient αSyn protein clearance [70–73]. The plot of the αSyn clearance assay via
410 western blot immunodetection in the presence of 100 μM of JWH-018 over a 12-hour
411 period revealed higher αSyn levels in the presence of JWH-018 compared to the control
412 at time point 9h ($p<0.1$) (Fig. 3a), and different αSyn-GFP levels in the Δ6-0, Δ9-6, and
413 Δ12-9 time intervals (Fig. 3b). This result points towards a statistically significant
414 difference in αSyn-GFP clearance rate in the presence of 100 μM of JWH-018 at the Δ9-
415 6 time interval, which only decreased by 16±7% ($P<0.02$) in contrast with 31±3% in
416 untreated cells, representing almost a 50% clearance rate decrease between both
417 conditions. This change in αSyn-GFP clearance in the presence of the synthetic
418 cannabinoid can justify the increment of αSyn protein levels.

419

420 This decrease in αSyn-GFP clearance upon incubation with JWH-018 could stem
421 from the dysfunction of the cellular mechanisms involved in this process. αSyn
422 accumulation has been linked to dysfunction in protein degradation, namely in the UPS
423 and the autophagy-lysosomal pathway [70–73]. Like in human cells, αSyn can be degraded
424 via the ubiquitin-proteasome system and autophagy in *S. cerevisiae* [74]. However, the
425 contribution of the proteasome system in αSyn clearance seems to be lower than by
426 autophagy/vacuole, at least in yeast models of PD [75]. The effect of the incubation of 100
427 μM of JWH-018 on the UPS of αSyn-expressing yeast cells was assessed via the co-
428 expression of an unstable, proteasome-degradable form of GFP – GFPu [56,57]. The
429 Western-blot assays showed a significant increment of 340 ± 110 % of GFPu protein

levels ($P<0.05$) after 14h in the presence of 100 µM of JWH-018 (Fig. 4a), corroborated by GFP fluorescence analyses that showed an increase of 43.1±17.57 % ($P<0.02$), compared to the control (cells incubated with 0 µM of compound) (Fig. 4b). Concomitantly, αSyn levels increased in a similar fashion ($P<0.05$) (Fig. 4a). These assays point towards a dysregulation of the ubiquitin-proteasome pathway, affecting the clearance rate of αSyn. To our knowledge, this is the first study describing a link between the dysregulation of this system and synthetic cannabinoids. Phytocannabinoid Δ^9-tetrahydrocannabinol induced a significant decrease of proteasome function in the brain by decreasing 20S proteasome chymotrypsin-like protease activity [76]. Furthermore, the 20S proteasome complex is ATP-dependent, and in yeast, ATP is essential for multiple steps in proteasome function; which renders its activity directly proportional to the amount of ATP in cells [77], namely in *S. cerevisiae,* where ubiquitin conjugation to substrates by E1 is an ATP-dependent step [78]. In this study, we observed that cells incubated with 100 µM of JWH-018 showed a higher ATP content than the untreated control (Fig 1e), giving the hypothesis that ATP is being accumulated as a consequence of proteasome function impairment. Although this observation is seemingly paradoxical, since it has been well established that ATP concentration directly influences proteasome activity [79–81], certain studies have described a tandem increase in ATP production with an impairment of proteasome function in a yeast proteasome impairment model strain, which produces a mutated form of the 20S catalytic unit of the protein degradation complex. This finding brings to light an interplay between mitochondrial function and the proteasome, particularly under oxidative stress conditions [82]. Moreover, recent studies also indicate that proteasome function can be preserved even under acute and prolonged glucose starvation (with consequent decrease in cellular ATP levels) [83], which leads to

454 the hypothesis that the dependence between proteasome function and intracellular ATP
455 levels may not be as clear-cut as anticipated.
456
457 The results indicate a decrease in UPS activity in the presence of 100 μM of JWH-
458 018, resulting in the accumulation of αSyn. We also investigated autophagy, since this
459 mechanism is also known to be involved in protein clearance, and has been described to
460 be upregulated as a compensatory mechanism to deal with αSyn excess [84]. Autophagy
461 induction was studied by western blot densitometric analysis using GFP-Atg8 as a
462 reporter [57,58].. Our results showed Atg8 induction and autophagic flux results were
463 similar in the presence or absence of 100 μM of JWH-018. αSyn was also analysed, and
464 as expected, a significant increment in its concentration was observed in the presence of
465 JWH-018 ($P<0.02$). Nevertheless, a starvation condition was included as a positive
466 control and, as expected, autophagy increased compared with the control culture
467 ($P<0.01$); concomitantly, αSyn levels decreased by 53.5 ± 15,2 % ($P<0.05$). There are no
468 scientific studies correlating autophagy with synthetic cannabinoids, only studies
469 involving phytocannabinoids and cancer cells, suggesting that natural compounds induce
470 autophagy mechanisms leading to cell death [85–87].
471

472 ***Final considerations***

473 In summary, the yeast model of PD was used to understand the possible protective
474 or toxic roles of synthetic cannabinoid JWH-018 in PD. Cells treated with the synthetic
475 cannabinoid showed increased αSyn toxicity and a decrease in the final biomass.
476 Moreover, treatment with 100 μM JWH-018 increased αSyn protein levels and increased
477 formation of αSyn-GFP inclusions. The dysregulation of αSyn clearance in the presence

of 100μM JWH-018 was evaluated, revealing an impairment of the ubiquitin-proteasome system.

The results obtained here open new and interesting hypotheses for future work, and will require complementary approaches. To the best of our knowledge, this study constitutes the first approach to using a yeast PD model to investigate the effects of SCs in PD and its underlying molecular mechanisms.

Experimental Procedures

Tested compound

Selected synthetic cannabinoid was JWH-018 [1-naphthalenyl(1-pentyl-1H-indol-3-yl)-methanone]. JWH-018 was obtained as >98.5% pure powder from Lipomed AG, Switzerland. Stock solutions of this compound were prepared in 100% DMSO in different concentrations: 0.25 mM, 2.50 mM, 12.50 mM, 18.75 mM, and 25.00 mM, and tested in yeast cultures at a final DMSO concentration of 0.4%.

Cell culture

The study was performed using *S. cerevisiae* BY4741 cells ((*MATa; his3*Δ*1; leu2*Δ*0; met15*Δ*0; ura3*Δ*0*) obtained from Euroscarf collection (Frankfurt, Germany). The yeast expression vector pRS426-GAL was used to express a human αSyn-GFP fusion under a galactose-inducible promoter (*GAL*), pRS426GAL αSyn-GFP, as described before [56]. Other plasmids used included: (i) pRS413GPD-GFPu, expressing an unstable GFP under the regulation of *GPD* constitutive promoter to study the proteasome [88], and (ii)

pRS415_GFP-ATG8, to study autophagy [88]. When relevant, cells transformed with the empty plasmids (pRS426GAL, pRS413-GPD, or pRS415) were used as control.

Cells transformed with either pRS426GAL-αSyn-GFP or pRS426GAL were grown in synthetic complete (SC) medium without uracil (SC-Ura); cells co-transformed with pRS426GAL-αSyn and pRS413-GPD-GFPu in SC medium without uracil nor histidine (SC-Ura-His); and cells transformed with pRS415_GFP-ATG8 in SC medium without uracil nor leucine (SC-Ura-Leu) [0.67% (w/v) Yeast Nitrogen Base (BD Biosciences) + appropriate amino acid dropout mix (Sunrise Science Products). Yeast cells were pre-grown in SC-Ura containing 1% (w/v) raffinose at 30◦C, with orbital shaking (200 rpm) for 24 h, and subsequently diluted to an OD_{600} of 2×10^{-3} after overnight growth in the same medium. After 24 hours, new cultures were prepared to an initial standardised OD_{600} = 0.03 in SC-Ura containing 1 % (w/v) galactose under the same conditions to induce the overexpression of proteins under the *GAL* promoter. For the clearance assays, after 14h of αSyn-GFP expression induction (in the presence of 0 or 100 μM of the synthetic cannabinoid), cells were collected by centrifugation, washed in PBS, resuspended in SC medium with 2% (w/v) glucose to repress αSyn expression, and incubated for 12h at 30°C. αSyn levels were determined by western blotting at 14 h of induction (i.e. immediately prior to growth medium change, corresponding to 0 h of clearance), and after 6, 9, and 12 h post growth medium change. The αSyn-GFP clearance kinetics were determined using the procedure described in [55] for monophasic decay. Briefly, the half-lives of αSyn-GFP were extrapolated from the Western-blot study by regression analyses assuming that the decay of α-Syn follows a monophasic exponential decay [$y = f(e^{-kx})$]. The positive control (C+ in Figure 4) corresponds to aliquots of cells collected after 8 hours of clearance.

Growth kinetics

The cytotoxic properties of JWH-018 were assessed via cell growth kinetics in the presence of 0 µM, 1 µM, 10 µM, 50 µM, 75 µM or 100 µM of JWH-018. Growth analysis was monitored for 24 hours using a ELX808U thermostatic microplate reader (Biotek), with the temperature set to 30◦C and the wavelength set to 600 nm, with readings collected hourly by Gene5 data analysis software. Growth curves were fitted to the standard form of the logistic growth equation using Graphpad Prism software, after subtraction of the minimum value. The parameters extracted from the fitted results were the final biomass and the growth rate. The doubling time (DT) value was computed from the growth rate (k) using the formula Ln2/k.

MTT assay

This assay was performed to determine mitochondrial activity after incubation with JWH-018. Cells overexpressing αSyn-GFP or transformed with the empty vector were exposed to 10 or 100 µM of JWH-018 and analysed during the lag, initial log, and final log phases (corresponding to 6h, 10h, and 14h for the lower SC concentration, and 3h, 7h, and 10h for the higher). Aliquots of 1,5 mL (for the lag phase) or 1 mL (for the initial log and final log phases) were collected and washed with water; cells were subsequently exposed to 3-(4,5-dimethylthiazol-2-yl)-2,5-diphenyltetrazolium bromide (MTT) (0.5 mg/mL) for 4h at 30 ºC. Aliquots were then centrifuged, and crystals were resuspended in 150µL of DMSO. After homogenisation, the optical density was recorded at 492 nm in a microplate reader and corrected for the cell density. In all experiments, the value obtained from untreated cell culture controls was set as corresponding to 100% cell viability.

549 ***Superoxide quantification***

550 Superoxide quantification was performed using fluorescent dihydroethidium
551 (hydroethidine) (Life Technologies). BY4741 yeast cells transformed with p426GAL-
552 αSyn-GFP or p426Gal were exposed to 10 or 100 μM of JWH-018. Aliquots of 2.0 mL
553 from each cell growth phase were collected and incubated with 10 μM of hydroethidine
554 for 1.5 hours at 30 °C under shaking (150 rpm). Samples were subsequently centrifuged
555 for 3 min at 10 000 × *g*, and the resulting pellets were washed with sterile water and
556 resuspended in 100 μL of water. The fluorescence was measured (λ_{ex} = 358 nm, λ_{em} =
557 460 nm), and corrected for the cell density in the samples.
558

559 ***ATP quantification***

560 The ATP Colorimetric/Fluorometric assay kit from Sigma-Aldrich was used to
561 quantify ATP in cell samples collected during the final log phase. To test the effect of
562 JWH-018, cells transformed with p426GAL or p426Gal-αSyn-GFP were used. Cells were
563 exposed to 10 or 100 μM of JWH-018. 1000 μL of culture samples were treated as
564 described in a previous publication [53]. ATP quantification was performed according to
565 conditions described under colorimetric detection. Protein quantification was performed
566 using Bio-Rad protein assay dye reagent concentrate to normalise the ATP quantification
567 values.
568

569 ***Fluorescence microscopy***

570 The percentage of cells with αSyn inclusions after exposure to JWH-018 was
571 determined by fluorescence microscopy. Yeast cells were grown as described above for
572 14h, and subsequently collected by centrifugation, resuspended in PBS, added to a

573 microscope slide, and analysed using a Zeiss Axiovert 200 M (Carl Zeiss) widefield
574 fluorescence microscope equipped with a cooled CCD camera (Roper Scientific
575 Coolsnap HQ). A minimum of 150 cells were manually counted using ImageJ (NIH,
576 Bethesda, Md, USA) for each biological replicate. GFP fluorescence was detected using
577 an Ar laser's 488 nm laser line (25 mW nominal output) and a custom wavelength
578 detection window set to 493–556 nm.
579

580 ***Protein extraction and western blot analysis***

581 For total protein extraction, yeast cells were lysed in Tris-HCl buffer pH 7.6
582 supplemented with a protease and phosphatase inhibitor cocktail (Roche, Mannheim,
583 Germany), with glass beads and subjected to 3 cycles of 30 seconds in a bead beater and
584 1 min on ice. Cell debris was removed by centrifugation (700 × *g*, 3 min, 4ºC), and the
585 supernatant was collected. Protein concentration was determined using the BCA protein
586 assay kit (Thermo Fisher Scientific Inc, Illinois, USA). 20 µg of total protein was loaded
587 in the SDS-PAGE. Protein sample buffer (200 mM Tris-HCl pH 6.8, 6% 2-
588 mercaptoethanol, 8% SDS, 40% glycerol, 0.4% bromophenol blue) was added to each
589 protein sample and heated for 10 min at 100ºC before gel loading. Protein samples were
590 run in SDS-PAGE and subsequently transferred to a nitrocellulose membrane using a
591 Trans-Blot Turbo transfer system (Bio-Rad), according to the manufacturer's
592 specifications. Immunoblotting was performed following standard procedures with the
593 following antibodies: anti-αSyn (BD Transduction Laboratories, San Jose, CA, USA),
594 anti-pS129-αSyn (Wako Chemicals USA, Inc., Richmond VA, USA), and anti-GFP
595 (SICGEN AB0066-200, Cantanhede, Portugal). Anti-Pgk1 (NovexTM, Rockford, USA)
596 was used as the loading control. Antibodies were diluted to 1:1000 (anti-αSyn), 1:4000
597 (anti-pS129-αSyn), 1:2500 (anti-GFP), and 1:2000 (anti-Pgk1) in PBS. The secondary

antibodies used were anti-mouse (HRP) and anti-goat (HRP) diluted to 1:5000. The band intensity of the different immunoblot signals was estimated using ImageJ software and normalised against the Pgk1 signal. In particular, αSyn levels were determined by calculating the αSyn/Pgk1 ratio, and normalised to the control condition; pS129-αSyn levels were determined by calculating the ratio between both values: (pS129/Pgk1)/(αSyn/Pgk1) and normalised to the control condition; GFPu levels were determined by calculating the GFP/Pgk1 ratio, and normalised to the control condition; Atg8 induction was quantified by calculating the fold increase of total GFP signal (GFP-Atg8 and free GFP signal, detected with anti-GFP) normalised to Pgk1, and normalised to the control condition; and autophagic flux was determined by measuring the vacuolar degradation of the Atg8 domain reporter (freeGFP/totalGFP)/Pgk1, and normalised to the control. The results were obtained from at least three independent experiments with similar outcomes. Full-length, uncropped blots are presented in Supplementary Figs. S1–S4.

GFP Fluorescence assessment by spectrofluorometry

GFP fluorescence was assessed by spectrofluorometry (Perkin Elmer LS50B spectrofluorometer) in BY4741 cells co-transformed with pRS426GAL-αSyn and pRS413-GPD-GFPu. Cells were exposed to 100 µM of JWH-018 and allowed to grow for 14h under the aforementioned conditions, after which 2 mL of each culture were collected and centrifuged for 3 min at 10 000 × *g*. The resulting pellets were washed with sterile water, and resuspended in 100 µL of water. The fluorescence was measured (λ_{ex} = 475 nm, λ_{em} = 520 nm), and corrected for the cell density in the samples.

Statistical analysis

Statistical analysis was performed using an unpaired two-tailed *t*-test. P-value < 0.05 was considered statistically significant. Statistics were performed using Prism 8 (GraphPad Software Inc.).

References

1. Ho, M. S. Clearance Pathways for α-Synuclein in Parkinson's Disease. *J. Neurochem.* **169**, e70124 (2025).
2. Kulcsarova, K., Skorvanek, M., Postuma, R. B. & Berg, D. Defining Parkinson's Disease: Past and Future. *Journal of Parkinson's Disease* vol. 14 Preprint at https://doi.org/10.3233/JPD-230411 (2024).
3. Cao, Z. *et al.* Excitation-inhibition balance abnormally shapes structure–function coupling of gray matter in Parkinson's disease. *NPJ Parkinsons Dis.* **11**, 168 (2025).
4. Arias-Carrión, O., Guerra-Crespo, M., Padilla-Godínez, F. J., Soto-Rojas, L. O. & Manjarrez, E. α-Synuclein Pathology in Synucleinopathies: Mechanisms, Biomarkers, and Therapeutic Challenges. *International Journal of Molecular Sciences 2025, Vol. 26, Page 5405* **26**, 5405 (2025).
5. Sharma, M. & Burré, J. α-Synuclein in synaptic function and dysfunction. *Trends Neurosci.* **46**, 153–166 (2023).
6. Deng, H. & Yuan, L. Genetic variants and animal models in SNCA and Parkinson disease. *Ageing Res. Rev.* **15**, 161–176 (2014).
7. Mohammadi, R. *et al.* Common SNCA Genetic Variants and Parkinson's Disease Risk: A Systematic Review and Meta-Analysis. *Int. J. Mol. Sci.* **26**, (2025).
8. Gao, V., Briano, J. A., Komer, L. E. & Burré, J. Functional and Pathological Effects of α-Synuclein on Synaptic SNARE Complexes. *J. Mol. Biol.* **435**, 167714 (2023).
9. Dias, S. B. *et al.* Age-Related Changes of the Synucleins Profile in the Mouse Retina. *Biomolecules* **13**, 180 (2023).
10. Park, H., Kam, T. I., Dawson, V. L. & Dawson, T. M. α-Synuclein pathology as a target in neurodegenerative diseases. *Nature Reviews Neurology* vol. 21 Preprint at https://doi.org/10.1038/s41582-024-01043-w (2025).
11. Flores-León, M. & Outeiro, T. F. Expanding our understanding of synucleinopathies: proteinopathy, proteinopenia, and lipidopathy. *FEBS Journal* https://doi.org/10.1111/FEBS.70011;REQUESTEDJOURNAL:JOURNAL:17424658;WGROUP:STRING:PUBLICATION (2025) doi:10.1111/FEBS.70011;REQUESTEDJOURNAL:JOURNAL:17424658;WGROUP:STRING:PUBLICATION.
12. Fanning, S. & Selkoe, D. Parkinson disease is a fatty acidopathy. *Nat. Rev. Neurol.* **21**, 642–655 (2025).
13. Tu, R. *et al.* From pathogenesis to treatment: the emerging role of ferroptosis in Parkinson's disease. *Front. Immunol.* **16**, (2025).
14. Espay, A. J. & Lees, A. J. Loss of monomeric alpha-synuclein (synucleinopenia) and the origin of Parkinson's disease. *Parkinsonism Relat. Disord.* **122**, 106077 (2024).

15. Ferreira, C., Almeida, C., Tenreiro, S. & Quintas, A. Neuroprotection or Neurotoxicity of Illicit Drugs on Parkinson's Disease. *Life (Basel)* **10**, 86 (2020).
16. Menozzi, E. & Schapira, A. H. V. Prospects for Disease Slowing in Parkinson Disease. *Annu. Rev. Pharmacol. Toxicol.* **65**, 237–258 (2025).
17. de Freitas, M. E. T. & Fox, S. H. Advice to People with Parkinson's in My Clinic: Cannabis. *J. Parkinsons Dis.* **14**, 873–881 (2024).
18. Feeney, M. P. *et al.* Weeding through the haze: a survey on cannabis use among people living with Parkinson's disease in the US. *NPJ Parkinsons Dis.* **7**, 21 (2021).
19. Holden, S. K., Domen, C. H., Sillau, S., Liu, Y. & Leehey, M. A. Higher Risk, Higher Reward? Self-Reported Effects of Real-World Cannabis Use in Parkinson's Disease. *Mov. Disord. Clin. Pract.* **9**, 340–350 (2022).
20. Alves, A. de D. F., Dias, F. C. R., Cadena, P. G. & Silva-Jr, V. A. Use of phytocanabinoids in animal models of Parkinson's disease: Systematic review. *Neurotoxicology* **105**, 34–44 (2024).
21. Martinotti, G. *et al.* Synthetic Cannabinoids: Psychopharmacology, Clinical Aspects, Psychotic Onset. *CNS Neurol. Disord. Drug Targets* **16**, 567–575 (2017).
22. Fernández-Ruiz, J., Romero, J. & Ramos, J. A. Endocannabinoids and Neurodegenerative Disorders: Parkinson's Disease, Huntington's Chorea, Alzheimer's Disease, and Others. *Handb. Exp. Pharmacol.* **231**, 233–59 (2015).
23. Villanueva, E. B., Little, J. P. & Klegeris, A. Therapeutic Potential of Cannabinoids in the Treatment of Neuroinflammation Associated with Parkinson's Disease. in *Recent Advances in Medicinal Chemistry* 59–75 (BENTHAM SCIENCE PUBLISHERS, 2015). doi:10.2174/9781681081717115020005.
24. Basavarajappa, B. S., Shivakumar, M., Joshi, V. & Subbanna, S. Endocannabinoid system in neurodegenerative disorders. *J. Neurochem.* **142**, 624–648 (2017).
25. Gowran, A., Noonan, J. & Campbell, V. A. The Multiplicity of Action of Cannabinoids: Implications for Treating Neurodegeneration. *CNS Neurosci. Ther.* **17**, 637–644 (2011).
26. Ferreira, C., Almeida, C., Tenreiro, S. & Quintas, A. Neuroprotection or Neurotoxicity of Illicit Drugs on Parkinson's Disease. . **10**, 86 (2020).
27. Basavarajappa, B. S., Shivakumar, M., Joshi, V. & Subbanna, S. Endocannabinoid system in neurodegenerative disorders. *J. Neurochem.* **142**, 624–648 (2017).
28. Chung, Y. C. *et al.* CB2 receptor activation prevents glial-derived neurotoxic mediator production, BBB leakage and peripheral immune cell infiltration and rescues dopamine neurons in the MPTP model of Parkinson's disease. *Exp. Mol. Med.* **48**, e205–e205 (2016).
29. De Luca, M. A. & Fattore, L. Therapeutic Use of Synthetic Cannabinoids: Still an Open Issue? *Clin. Ther.* **40**, 1457–1466 (2018).
30. Neoh, M. J. Y. *et al.* The novel psychoactive substances epidemic: A scientometric perspective. *Addiction Neuroscience* **5**, 100060 (2023).
31. Jerry, J., Collins, G. & Streem, D. Synthetic legal intoxicating drugs: the emerging 'incense' and 'bath salt' phenomenon. *Cleve. Clin. J. Med.* **79**, 258–64 (2012).
32. Omer, T. A. & Doherty, C. Posterior reversible encephalopathy syndrome (PRES) complicating the 'legal high' mephedrone. *Case Reports* **2011**, bcr0220113904–bcr0220113904 (2011).
33. Baumann, M. H. *et al.* The Designer Methcathinone Analogs, Mephedrone and Methylone, are Substrates for Monoamine Transporters in Brain Tissue. *Neuropsychopharmacology* **37**, 1192–1203 (2012).

34. Soares, J. *et al.* Structure-cytotoxicity relationship profile of 13 synthetic cathinones in differentiated human SH-SY5Y neuronal cells. *Neurotoxicology* **75**, 158–173 (2019).
35. Soares, J. *et al.* Adverse outcome pathways induced by 3,4-dimethylmethcathinone and 4-methylmethcathinone in differentiated human SH-SY5Y neuronal cells. *Arch. Toxicol.* **94**, 2481–2503 (2020).
36. Leong, H. S., Philp, M., Simone, M., Witting, P. K. & Fu, S. Synthetic Cathinones Induce Cell Death in Dopaminergic SH-SY5Y Cells via Stimulating Mitochondrial Dysfunction. *Int. J. Mol. Sci.* **21**, 1370 (2020).
37. de Mello-Sampayo, C. *et al.* Designer Cathinones N-Ethylhexedrone and Buphedrone Show Different In Vitro Neurotoxicity and Mice Behaviour Impairment. *Neurotox. Res.* **39**, 392–412 (2021).
38. Buzhdygan, T. P. *et al.* The psychoactive drug of abuse mephedrone differentially disrupts blood-brain barrier properties. *J. Neuroinflammation* **18**, 63 (2021).
39. Campeão, M. *et al.* Acute MDPV Binge Paradigm on Mice Emotional Behavior and Glial Signature. *Pharmaceuticals* **14**, 271 (2021).
40. Valente, M. J. *et al.* Neurotoxicity of β-Keto Amphetamines: Deathly Mechanisms Elicited by Methylone and MDPV in Human Dopaminergic SH-SY5Y Cells. *ACS Chem. Neurosci.* **8**, 850–859 (2017).
41. Coccini, T., Vecchio, S., Crevani, M. & De Simone, U. Cytotoxic Effects of 3,4-Catechol-PV (One Major MDPV Metabolite) on Human Dopaminergic SH-SY5Y Cells. *Neurotox. Res.* **35**, 49–62 (2019).
42. Siedlecka-Kroplewska, K., Wrońska, A., Stasiłojć, G. & Kmieć, Z. The Designer Drug 3-Fluoromethcathinone Induces Oxidative Stress and Activates Autophagy in HT22 Neuronal Cells. *Neurotox. Res.* **34**, 388–400 (2018).
43. Siedlecka-Kroplewska, K., Szczerba, A., Lipinska, A., Slebioda, T. & Kmiec, Z. 3-Fluoromethcathinone, a structural analog of mephedrone, inhibits growth and induces cell cycle arrest in HT22 mouse hippocampal cells. *J. Physiol. Pharmacol.* **65**, 241–6 (2014).
44. Giorgetti, A. *et al.* Molecular Mechanisms of Action of Novel Psychoactive Substances (NPS). A New Threat for Young Drug Users with Forensic-Toxicological Implications. *Life (Basel)* **11**, (2021).
45. European Monitoring Centre for Drugs and Drug Addiction. *European Drug Report 2021: Trends and Developments*. (2021) doi:10.2810/18539.
46. Menezes, R., Tenreiro, S., Macedo, D., Santos, C. & Outeiro, T. From the baker to the bedside: yeast models of Parkinson's disease. *Microbial Cell* **2**, 262–279 (2015).
47. Tenreiro, S., Munder, M. C., Alberti, S. & Outeiro, T. F. Harnessing the power of yeast to unravel the molecular basis of neurodegeneration. *J. Neurochem.* **127**, 438–452 (2013).
48. Tenreiro, S. & Outeiro, T. F. Simple is good: yeast models of neurodegeneration. *FEMS Yeast Res.* **10**, 970–979 (2010).
49. Tenreiro, S., Franssens, V., Winderickx, J. & Outeiro, T. F. Yeast models of Parkinson's disease-associated molecular pathologies. *Curr. Opin. Genet. Dev.* **44**, 74–83 (2017).
50. Atwood, B. K., Huffman, J., Straiker, A. & MacKie, K. JWH018, a common constituent of 'Spice' herbal blends, is a potent and efficacious cannabinoid CB1 receptor agonist. *Br. J. Pharmacol.* **160**, 585 (2010).
51. Ferreira, C., Almeida, C., Tenreiro, S. & Quintas, A. Neuroprotection or Neurotoxicity of Illicit Drugs on Parkinson's Disease. . **10**, 86 (2020).

52. McLean, P. J., Kawamata, H. & Hyman, B. T. Alpha-synuclein-enhanced green fluorescent protein fusion proteins form proteasome sensitive inclusions in primary neurons. *Neuroscience* **104**, 901–12 (2001).
53. Ferreira, C. *et al.* The synthetic cannabinoid JWH-018 modulates Saccharomyces cerevisiae energetic metabolism. *FEMS Yeast Res.* **19**, 1–11 (2019).
54. Oueslati, A. Implication of Alpha-Synuclein Phosphorylation at S129 in Synucleinopathies: What Have We Learned in the Last Decade? *J. Parkinsons Dis.* **6**, 39–51 (2016).
55. Li, W. *et al.* Stabilisation of alpha-synuclein protein with aging and familial parkinson's disease-linked A53T mutation. *J. Neurosci.* **24**, 7400–9 (2004).
56. Outeiro, T. F. & Lindquist, S. Yeast Cells Provide Insight into Alpha-Synuclein Biology and Pathobiology. *Science (1979).* **302**, 1772–1775 (2003).
57. Macedo, D. *et al.* (Poly)phenols protect from α-synuclein toxicity by reducing oxidative stress and promoting autophagy. *Hum. Mol. Genet.* **24**, 1717–1732 (2015).
58. Lee, F. K. M. *et al.* The role of ubiquitin linkages on α-synuclein induced-toxicity in a Drosophila model of Parkinson's disease. *J. Neurochem.* **110**, 208–219 (2009).
59. Klionsky, D. J. *et al.* Guidelines for the use and interpretation of assays for monitoring autophagy (4th edition)1. *Autophagy* **17**, 1–382 (2021).
60. Shpilka, T., Weidberg, H., Pietrokovski, S. & Elazar, Z. Atg8: an autophagy-related ubiquitin-like protein family. *Genome Biol.* **12**, 226 (2011).
61. Weinstein, A. M., Rosca, P., Fattore, L. & London, E. D. Synthetic Cathinone and Cannabinoid Designer Drugs Pose a Major Risk for Public Health. *Front. Psychiatry* **8**, 156 (2017).
62. Roque-Bravo, R. *et al.* Synthetic Cannabinoids: A Pharmacological and Toxicological Overview. *Annu. Rev. Pharmacol. Toxicol.* **63**, 187–209 (2023).
63. Couceiro, J. *et al.* Toxicological impact of JWH-018 and its phase I metabolite N-(3-hydroxypentyl) on human cell lines. *Forensic Sci. Int.* **264**, 100–105 (2016).
64. Sezer, Y., Jannuzzi, A. T., Huestis, M. A. & Alpertunga, B. In vitro assessment of the cytotoxic, genotoxic and oxidative stress effects of the synthetic cannabinoid JWH-018 in human SH-SY5Y neuronal cells. *Toxicol. Res. (Camb).* **9**, 734–740 (2021).
65. Lagunas, R. Energy metabolism of Saccharomyces cerevisiae discrepancy between ATP balance and known metabolic functions. *Biochimica et Biophysica Acta (BBA) - Bioenergetics* **440**, 661–674 (1976).
66. Narkiewicz, J., Giachin, G. & Legname, G. In vitro aggregation assays for the characterisation of α-synuclein prion-like properties. *Prion* **8**, 19–32 (2014).
67. Buell, A. K. *et al.* Solution conditions determine the relative importance of nucleation and growth processes in α-synuclein aggregation. *Proc. Natl. Acad. Sci. U. S. A.* **111**, 7671–6 (2014).
68. Breydo, L., Wu, J. W. & Uversky, V. N. A-synuclein misfolding and Parkinson's disease. *Biochim. Biophys. Acta* **1822**, 261–85 (2012).
69. Anderson, J. P. *et al.* Phosphorylation of Ser-129 Is the Dominant Pathological Modification of α-Synuclein in Familial and Sporadic Lewy Body Disease. *Journal of Biological Chemistry* **281**, 29739–29752 (2006).
70. Ebrahimi-Fakhari, D., Wahlster, L. & McLean, P. J. Protein degradation pathways in Parkinson's disease: curse or blessing. *Acta Neuropathol.* **124**, 153–172 (2012).
71. Klucken, J. *et al.* Alpha-synuclein aggregation involves a bafilomycin A 1 - sensitive autophagy pathway. *Autophagy* **8**, 754–766 (2012).

72. Lee, H.-J. Clearance of -Synuclein Oligomeric Intermediates via the Lysosomal Degradation Pathway. *Journal of Neuroscience* **24**, 1888–1896 (2004).
73. Zondler, L. *et al.* Proteasome impairment by α-synuclein. *PLoS One* **12**, e0184040 (2017).
74. Braun, R. J. Ubiquitin-dependent proteolysis in yeast cells expressing neurotoxic proteins. *Front. Mol. Neurosci.* **8**, 2009–2011 (2015).
75. Petroi, D. *et al.* Aggregate Clearance of α-Synuclein in Saccharomyces cerevisiae Depends More on Autophagosome and Vacuole Function Than on the Proteasome. *Journal of Biological Chemistry* **287**, 27567–27579 (2012).
76. Salgado-Mendialdúa, V. *et al.* Δ9-tetrahydrocannabinol modulates the proteasome system in the brain. *Biochem. Pharmacol.* **157**, 159–168 (2018).
77. Peth, A., Nathan, J. A. & Goldberg, A. L. The ATP Costs and Time Required to Degrade Ubiquitinated Proteins by the 26 S Proteasome. *Journal of Biological Chemistry* **288**, 29215–29222 (2013).
78. Finley, D., Ulrich, H. D., Sommer, T. & Kaiser, P. The Ubiquitin–Proteasome System of Saccharomyces cerevisiae. *Genetics* **192**, 319–360 (2012).
79. Huang, H. *et al.* Physiological levels of ATP negatively regulate proteasome function. *Cell Res.* **20**, 1372–1385 (2010).
80. Takaine, M., Imamura, H. & Yoshida, S. High and stable ATP levels prevent aberrant intracellular protein aggregation in yeast. *Elife* **11**, (2022).
81. Avellaneda Penatti, N. M. *et al.* Decreased levels of Prx1 are associated with proteasome impairment and mitochondrial dysfunction in the yeast Saccharomyces cerevisiae. *Arch. Biochem. Biophys.* **768**, 110406 (2025).
82. Pravica, M. *et al.* Proteasome-dependent degradation and nucleus-vacuole junctions sustain proteostasis during acute glucose starvation. *bioRxiv* 2026.04.22.720209 (2026) doi:10.64898/2026.04.22.720209.
83. Tenreiro, S. *et al.* Phosphorylation Modulates Clearance of Alpha-Synuclein Inclusions in a Yeast Model of Parkinson's Disease. *PLoS Genet.* **10**, e1004302 (2014).
84. Lee, X. C., Werner, E. & Falasca, M. Molecular mechanism of autophagy and its regulation by cannabinoids in cancer. *Cancers (Basel).* **13**, 1–26 (2021).
85. Costa, L., Amaral, C., Teixeira, N., Correia-Da-Silva, G. & Fonseca, B. M. Cannabinoid-induced autophagy: Protective or death role? *Prostaglandins Other Lipid Mediat.* **122**, 54–63 (2016).
86. Vrechi, T. A. M. *et al.* Cannabidiol induces autophagy via ERK1/2 activation in neural cells. *Sci. Rep.* **11**, 5434 (2021).
87. Macedo, D. *et al.* (Poly)phenol-digested metabolites modulate alpha-synuclein toxicity by regulating proteostasis. *Sci. Rep.* **8**, 6965 (2018).

Acknowledgments

CiiEM is supported by FCT – Fundação para a Ciência e Tecnologia, I.P., under project reference UID/4585/2025 (https://doi.org/10.54499/UID/04584/2025); iNOVA4Health—Programa de Medicina Translacional is supported by FCT – Fundação para a Ciência e Tecnologia, I.P., under project references UID/PRR/04462/2025 (https://doi.org/10.54499/UID/PRR/04462/2025) and UID/PRR2/04462/2025

(https://doi.org/10.54499/UID/PRR2/04462/2025). The Associate Laboratory LS4FUTURE is supported by Fundação para a Ciência e a Tecnologia (FCT, Portugal) through the funding LA/P/0087/2020 (DOI 10.54499/LA/P/0087/2020). The authors would also like to acknowledge CiiEM for internal funding via the NEUROCALM2023 project.

Author Contributions

Carla Ferreira: Experimental work, 1st draft of the manuscript

Rui Almeida: Writing of the final manuscript, full revision of the results

Sandra Tenreiro: Conceptualisation, supervision and final revision of the manuscript

Alexandre Quintas: Conceptualization, funding, supervision and final revision of the manuscript

All authors reviewed the manuscript and approved its final version.

Data availability statement

Full-length uncropped western blot images are included in the Supplementary Information file. All other datasets generated and/or analysed during the current study are available from the corresponding author on reasonable request.

Competing interests

The authors declare no competing interests.

Figure Legends

Fig 1- JWH-018 toxicity assays on *S. cerevisiae* BY4741 cells harboring vector p426Gal-αSyn-GFP or p426Gal (control). (A) Growth curves of *S. cerevisiae* exposed to different concentrations of JWH-018. Inset represents the percentage of CFU of αSyn-expressing cells treated with different concentrations of JWH-018 after 5 hours of growth, compared to untreated cells (B)

885 growth curves were fitted to the standard form of the logistic equation which allowed an
886 estimation of the final biomass and doubling time values (Dt) from the growth rate using the
887 formulae Ln2/r;●,▲: cells transformed with the p426Gal vector; and ■,▼: cells transformed with
888 the p426Gal-αSyn-GFP vector. (C) Mitochondrial activity and (D) superoxide quantification in
889 the presence of 10 and 100µM of JWH-018 during the lag, initial log, and final log phases. (E)
890 ATP quantification in the presence of 10 and 100µM of JWH-018. Values represent the mean ±
891 SD, and the representative result is shown from at least three independent experiments. **p<0.02;
892 *p<0.05 and #p<0.1.

893 Fig 2 - Cellular impact of JWH-018 on the toxicity of αSyn. (A) Intracellular localisation of WT
894 αSyn-GFP, and percentage of BY4741 WT yeast cells containing αSyn-GFP inclusions, assessed
895 by fluorescence microscopy after 14 hours of αSyn-GFP expression induction (*** p<0.001) (left
896 panel), and the corresponding quantification of the percentage of cells with inclusions (right
897 panel). (B) Total and S129-phosphorylated αSyn protein levels were quantified by western blot
898 analysis of total protein extracts after 14h of αSyn-GFP expression (left panel). Densitometric
899 analysis of the immunodetection assay was expressed by the ratio between αSyn and Pgk1
900 (αSyn/PGK; left panel); S129-αSyn and Pgk1 (S129 αSyn/PGK)/(αSyn/PGK) – middle panel;
901 and S129-αSyn levels normalised to the control total αSyn levels (S129 αSyn/ αSyn total; right
902 panel). The representative results are calculated as the average of, a minimum of three replicates.
903 Values represent the mean ± SD. (*p<0.05). In (B), αSyn, pS129-αSyn and Pgk1 were detected
904 on separate membranes loaded with the same protein extracts and processed in parallel; each strip
905 shows two adjacent lanes cropped from a single membrane, and strips from different membranes
906 are separated by white space. Full-length blots are presented in Supplementary Fig. S1.

907

908 Fig 3 - JWH-018 affects αSyn-GFP clearance. (A) Clearance evaluated by αSyn-GFP protein
909 levels at time points 0, 6, 9, and 12h, assessed by western blot (left panel); densitometric
910 analysis of the immunodetection of αSyn relative to Pgk1, resulted in the possible decrease
911 of the clearance rate of αSyn levels in the presence of JWH-018 at time 9h (#p<0.1) (right

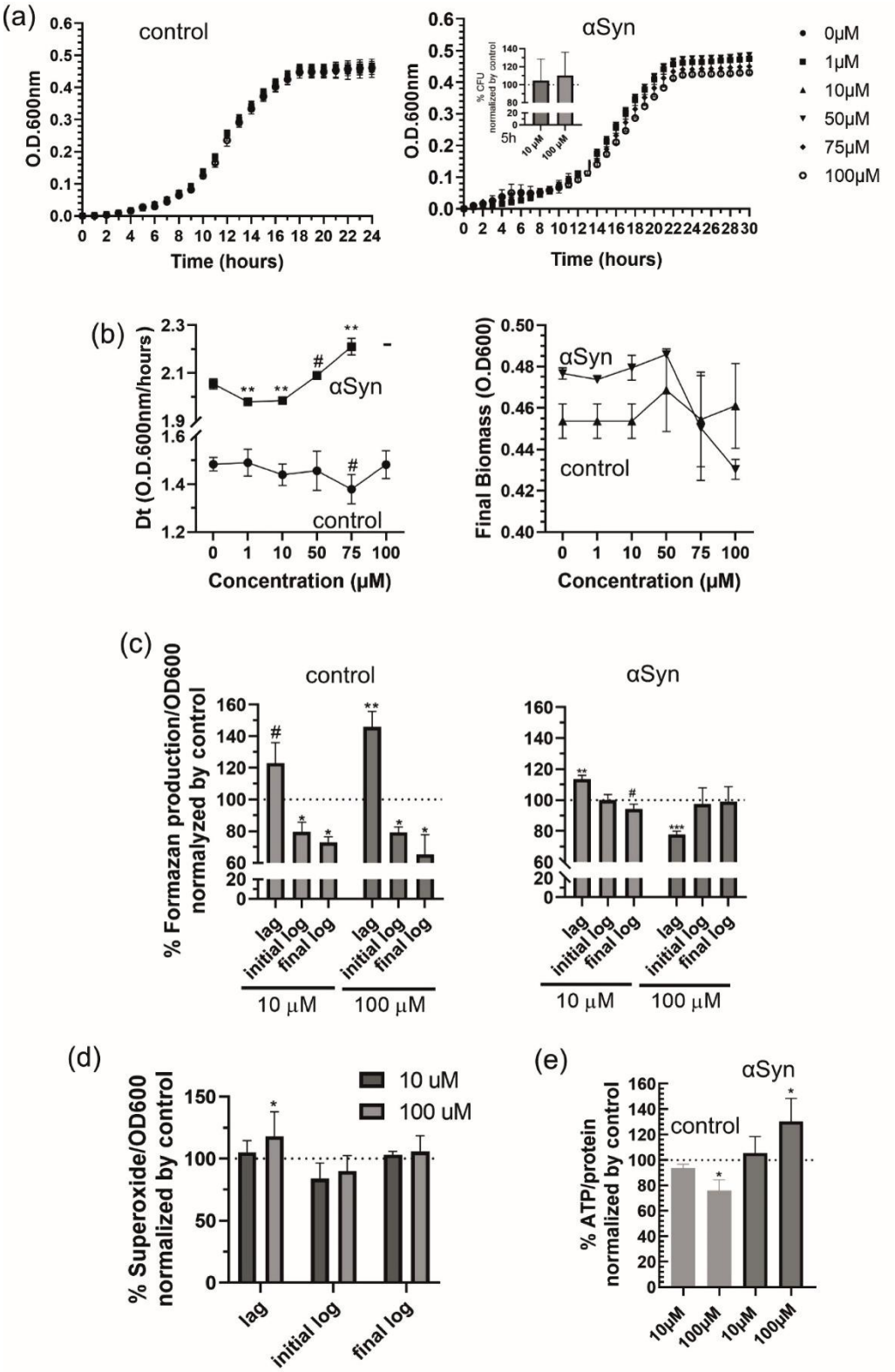
912 panel). (b) The kinetic degradation curve of αSyn suggests a possible increase in the
913 clearance rate of protein levels in JWH-018 presence when fitted to a one-phase exponential
914 decay. (c) Delta time points of αSyn clearance, resulting in a decrease of protein clearance
915 at time interval Δ9-6 in the presence of 100 μM of JWH-018 (*$p<0.05$). Each result
916 represents the average of three independent experiments. Values represent the mean ± SD.
917 In (A), αSyn and Pgk1 were detected on separate membranes loaded with the same protein
918 extracts and processed in parallel; each strip shows seven adjacent lanes cropped from a
919 single membrane, and strips from different membranes are separated by white space. Full-
920 length blots are presented in Supplementary Fig. S2.

921

922 Fig 4 - The JWH-018 impact on cellular protein degradation mechanisms. (A) GFPu and
923 αSyn protein levels were evaluated by western blot analysis of total protein extracts at 14h
924 and 18h (left panel), and their densitometric analysis relative to the loading control (Pgk1),
925 resulting in the accumulation of GFPu and αSyn in the presence of 100 μM of JWH-018
926 (*$p<0.05$) (right panel). (B) Spectrofluorometry of GFPu fluorescence shows a statistically
927 significant accumulation of GFPu in the presence of 100 μM of JWH-018 (*$p<0.05$). (C)
928 Autophagy evaluation via GFP-Atg8 protein levels calculated by western blot analysis of
929 total protein extracts at 14h (left-hand panel), and densitometric analysis of the
930 immunodetection of GFP and αSyn relative to the Pgk1 (right-hand panel). Representative
931 results are the average of three independent experiments. Values represent mean ± SD.
932 *$p<0.05$, **$p<0.02$; ***$p<0.01$ In (A) and (C), GFP (GFPu or GFP-Atg8/free GFP), αSyn
933 and Pgk1 were detected on separate membranes loaded with the same protein extracts and
934 processed in parallel; GFP-Atg8 and free GFP in (C) were detected on the same membrane.
935 Each strip shows adjacent lanes cropped from a single membrane (four lanes in A, three lanes
936 in C), and strips from different membranes are separated by white space. Full-length blots
937 are presented in Supplementary Figs. S3 (A) and S4 (C).

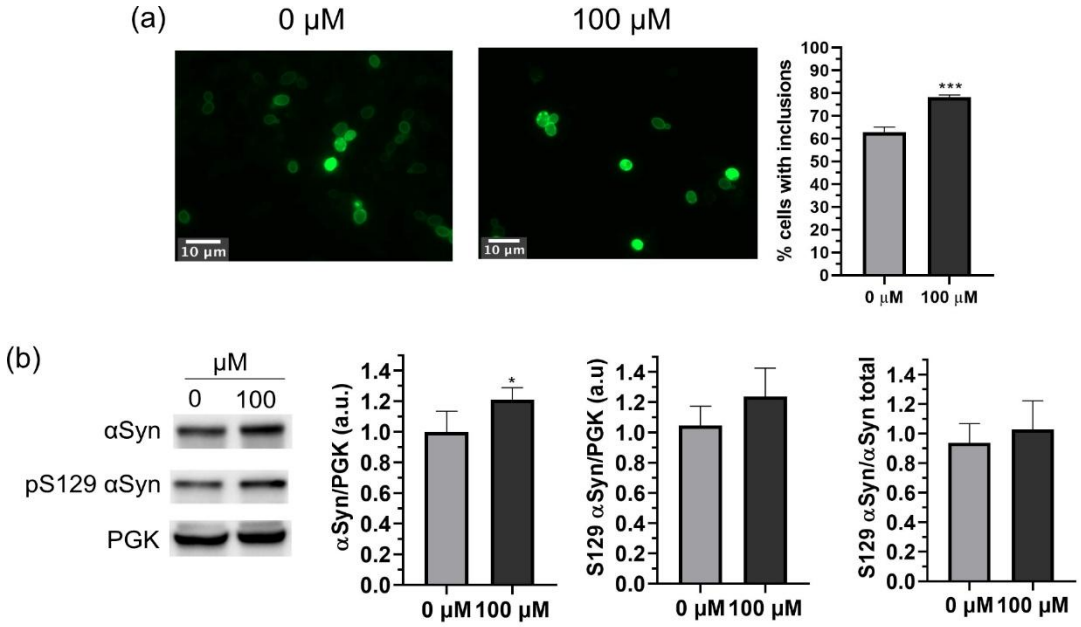
938

939 **Figure 1**



940

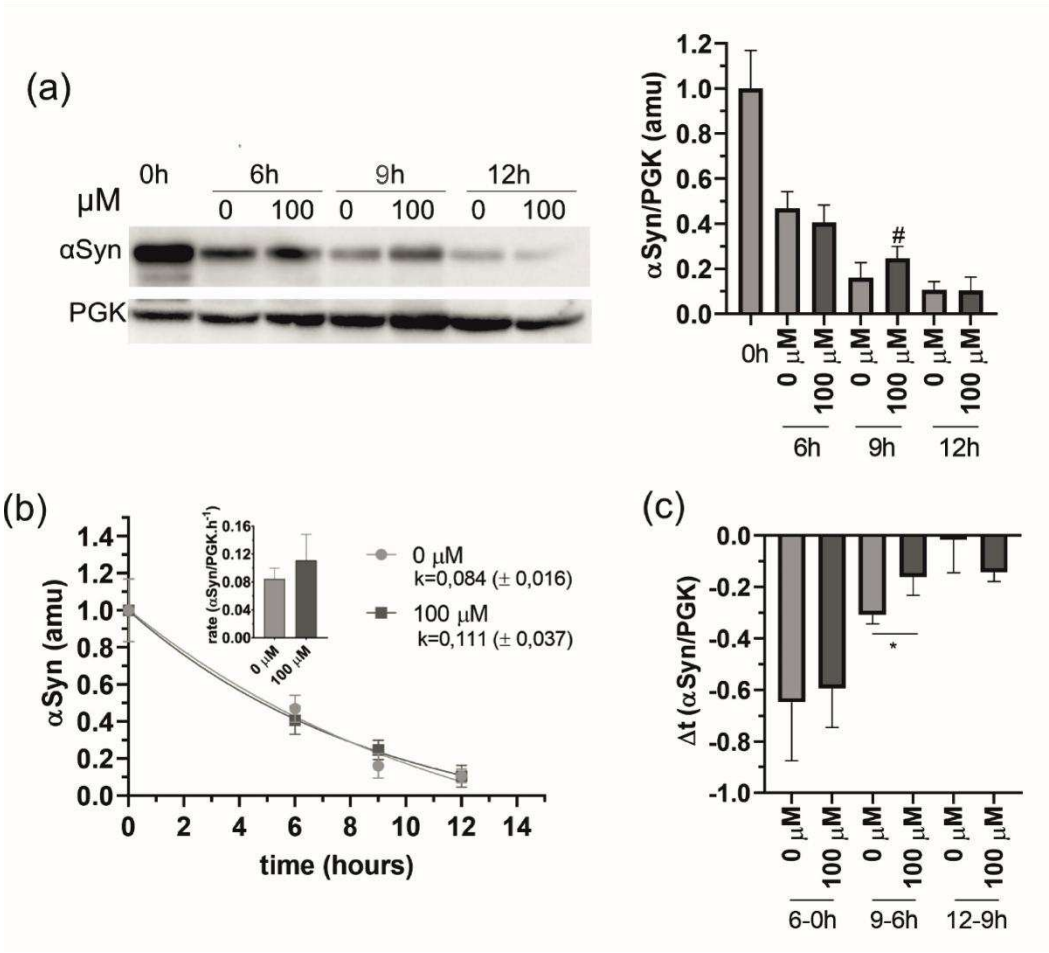
941 **Figure 2**



942

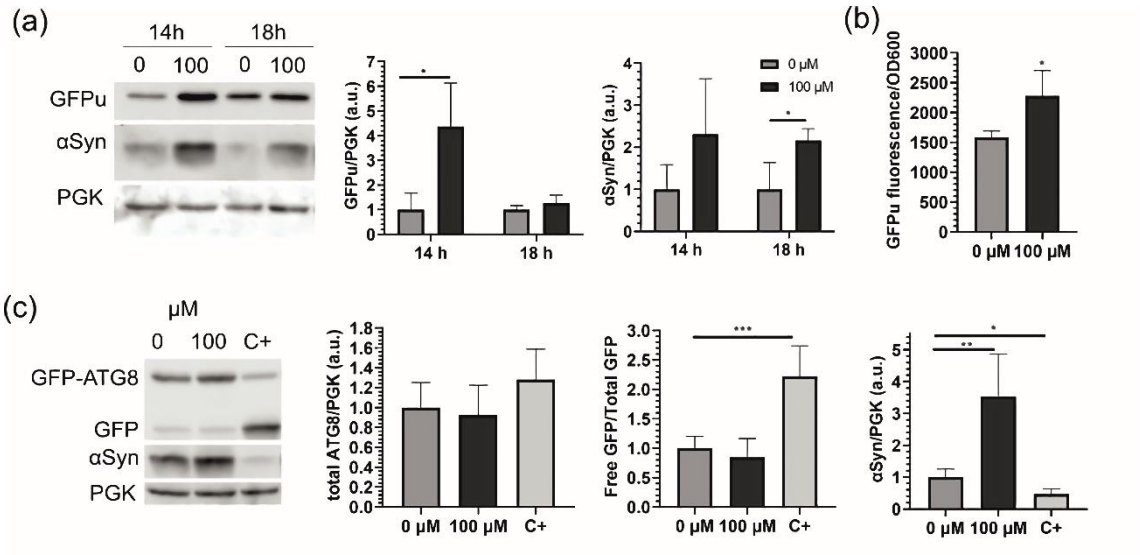
943

944 **Figure 3**



945

946 **Figure** **4**



947

Supplementary Files

This is a list of supplementary files associated with this preprint. Click to download.

- SupplementaryInformationWesternBlotsvs2.pdf